Misr J. Ag. Eng., 26(3): 1336- 1364 IRRIGATION AND DRAINAGE

THREE DIMENSION MODEL FOR SIMULATING INFILTRATION AND REDISTRIBUTION OF FURROW IRRIGATION WATER

A. El-Shafei[1]

ABSTRACT

Through redistribution, water which entered the soil during infiltration redistributes itself after infiltration has stopped. Both infiltration and redistribution profoundly affect soil water balance. The soil water balance determines the availability of water and nutrients to plants, affects rates of microbial processes, erosion, and chemical weathering, and influence soil thermal and gas composition relations. Therefore, three-dimensional finite difference model for simulating furrow surface flow, infiltration and redistribution water flow under both continuous and surged flow management was developed based on mass balance with the concept of matric flux potential and solved by the Newton-Raphson procedure. Model performance for both continuous and surge flow regimes was verified using field data. Three inflow cycle times ((5/5), (10/10) and (15/15)) were tested with three instantaneous flow rates of 1.45, 1.7 and 2.6 L/s, respectively. Field data were collected to evaluate the advance-recession time for stream flow along furrow length, field infiltration under different flow regimes and soil moisture distribution after irrigation. A sensitivity analysis was made on the response of the model to the changes in specific parameters. Application of the model to surge flow irrigation was demonstrated by analyzing some of the interrelationships between cycle times, flow rates, depth of application efficiency and distribution uniformity. The application efficiency was over 80 % by the surge flow, while it was about 48 % for the continuous flow. Infiltration rate under surge flow approached the basic infiltration in a short time compared to continuous flow. The result showed that a cycle (10/10 min) would create the best distribution uniformity (DU) and application efficiency (AE). The model accurately predicted the transient and steady soil moisture distribution under different inflow and furrow irrigation techniques.

[1]Asst. Prof., Ag. Eng. Dept., Fac. Ag., Alex. U.

INTRODUCTION

The Egyptian water budget is limited to the country's share of the Nile water, which is fixed according to international agreements and minor quantities of ground water and rainfall. Saving water is a national demand especially during these dry days depending on stored water back to the High Dam. In Egypt, an area of about 6 million feddans along the river sides and the Nile Delta were mainly irrigated by surface irrigation (Zin El-Abedin, 1988; Mohamed, 2007). Surface irrigation is the predominant method of irrigation around the world; among different surface water application techniques used in agricultural fields, furrow irrigation is mainly oriented to row crops. Thus, it is possible to invest some resources to improve furrow irrigation efficiency, specially when and where water resources are scarce (Mjelde et al. 1990). Infiltration is a direct function of time and place where it varies as these two parameters change (Childs et al., 1993). Oyonarte et al., (2002) explained the most important factors related to infiltration rate of water under irrigation conditions. Zapata and Playan (2000) reported that soil intake characteristics are described by experimental parameters in empirical infiltration equations or by soil properties in physically based infiltration equations. Spatial variability can be characterized by the frequency distribution of the infiltration parameters, but in certain cases it may also be necessary to determine spatial autocorrelation. Allen and Musick (2001) conducted study to evaluate the effects of deep ripping the lower 1/3 on irrigation infiltration, soil water storage and distribution, and grain yield along the furrow. Deep percolation and runoff are the main losses in furrow irrigation. To overcome this problem many ways such as surge irrigation, reuse of tailwater, cable irrigation and cutback methods have been tested and applied. Surge irrigation method was suggested by Stringham and keller (1979). Surging benefits reported on furrows can include faster water advance, increased infiltration uniformity, a reduction in the total volume of water required for an irrigation and less total irrigation time (Izuno and Podmore, 1985). Kassem and El-Tantawy (2000) studied the effect of off-time period in surge irrigation on total advance time, infiltration and irrigation efficiency. Mattar (2001) and Awady et al. (2005) showed that water application efficiency and

distribution uniformity increased under all surge flow treatments compared with continuous flow.

To enhance water application in furrow system, its design and operation must be based on quantitative relationships between soil hydrodynamic characteristics, and management of water and soil at a specific irrigated field. It is possible to evaluate the quality of an irrigation event (agronomic water efficiency components), by using mathematical relationships, simulation models or by direct measurements at experimental plots (Strelkoff and Souza, 1984). The quantitative analysis of furrow irrigation is obtained by the simultaneous solution of the Saint Venant and Richards equations (Gurovich, 1992). However, it is difficult to obtain analytic solutions for these equations, for specific soil hydrodynamic characteristics and different soil-water management combinations. Examples of mathematical models applied for the solution of Saint Venant and Richards equations have been published by Schwankl and Wallender (1988). Some methods developed for the simulation of furrow irrigation are based on the volume-balance approach, which is related to the continuity equation (Yu and Singh, 1990). Simulation modeling by numerical methods has been used to understand several surface water flow problems, and in many instances, simultaneous water infiltration-advance functions have been introduced in these models, as it occurs in field furrows. In most simulation modes, the water advance front (surface flow) and infiltration (sub-surface water flow) are represented by empiric equations, obtained from field measurements. High correlation of field experimental data with model simulation results (model validation) depend on the soil infiltration equation selected. In order to extrapolate the results obtained by using these simulation models to sites with different soil characteristics, parameters of the soil infiltration equations must be independent of the initial and boundary conditions (Hillel, 1980).

Many problems in infiltration and redistribution cannot be solved using one-dimensional models. Irrigation using furrow or trickle sources obviously must be described in terms of two or three dimensional flow. Analysis of a number of the methods used to measure hydraulic

properties, such as infiltrometers, also requires consideration of two or three dimensional flow fields (Campbell, 1985).

The objectives of this study were:

a) To develop a more realistic three dimensional finite difference model for simulating furrow infiltration and redistribution water flow under both continuous and surged flow management.
b) To test and verify the model under different independent variables such as inflow rate and irrigation cycle.
c) To set measures of comparison between predicted data and field data under continuous and surged flow management.

MATERIALS AND METHODS

Model Development

The present method used in analyzing three dimensional furrow infiltration and redistribution water flow was developed based on mass balance with the concept of matric flux potential and solved by the Newton-Raphson procedure. It was assumed that the soil is an isotropic homogeneous porous medium and soil-water movement was mainly isothermal, which neglects water movement in response to temperature gradient. Darcy's low applies in both saturated and unsaturated flow regions. The matrix flux potential; MFP (ϕ), which was introduced by Gardner (1958), was expressed as:

$$\phi = \int_{-\infty}^{\psi} k \, \mathrm{d}\psi \quad \text{----------(1)}$$

where: ψ : soil water potential (J kg^{-1}), and

k : unsaturated hydraulic conductivity (kg s m^{-3}).

MFP is suitable for less powerful computers and avoids arbitrary choices for element conductance by linearizing the problem. The use of ϕ as the driving force in the flow equation resulted in a linear equation for steady flow as presented by Campbell (1985)

$$f_i = -A\frac{\partial \phi_{i,j,k}}{\partial z} \quad \text{----------(2)}$$

where: f_i: water flux density in vertical direction; i (kg s^{-1}),

A: cross section area= $\Delta x \Delta y$ (m^2), and z: soil depth (m).

It is worth noting that when the mass balance approach is used to set up the simulation of water flow problem, it simplifies the governing partial differential equation; PDE. Direct approximation to the laws governing the physical system is applied locally to each cell control volume surrounding each grid point (Croft and Lilley, 1977). Figure. 1 shows node (*i*,*j*,*k*) surrounded by six nodes with their matric flux potentials (ϕ), fluxes caused by differences between matric flux potentials (*f's*) and fluxes caused by gravity (*U's*) in a 3-D cartesian coordinate region with uniform grid spacing (Δx, Δy and Δz).

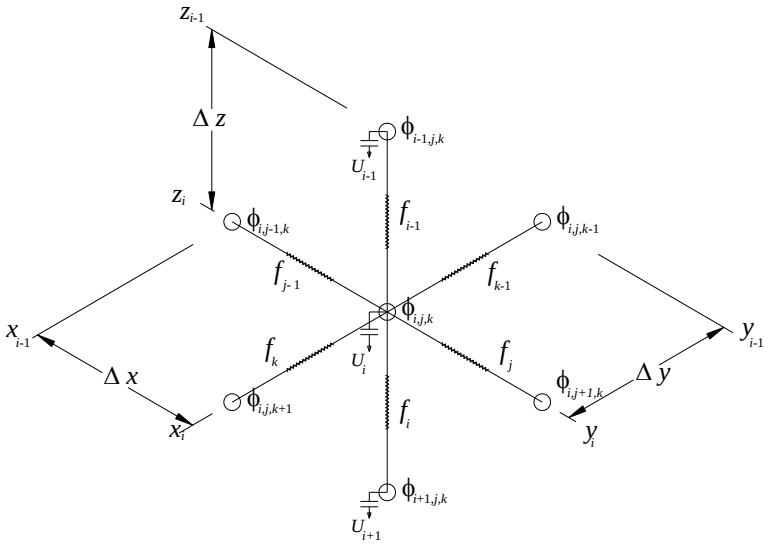

Figure. 1. Seven nodes, matric flux potentials (ϕ) and fluxes (*f's* and *U's*) for the Newton-Raphson calculation in a 3-D cartesian coordinate region with uniform grid spacing (Δx, Δy and Δz).

To apply this method to solution of three dimensional infiltration problem, the mass balance for node (*i*,*j*,*k*) was written in the following equation .

$$F_{i,j,k} = f_{i-1} - f_i + f_{j-1} - f_j + f_{k-1} - f_k + U_{i-1} - U_i + \frac{\rho_w \left(\theta_{i,j,k}^{t+1} - \theta_{i,j,k}^{t}\right)\Delta x \Delta y \Delta z}{\Delta t} \quad \text{----------(3)}$$

where:

$F_{i,j,k}$: net mass balance for node (*i*,*j*,*k*)

f_{i-1} & f_i : inlet and outlet fluxes through node (*i*,*j*,*k*) due to the difference matric flux potential in *z* direction (kg s^{-1}),

f_{j-1} & f_j : inlet and outlet fluxes through node (i,j,k) due to the difference matric flux potential in x direction (kg s^{-1}),
f_{k-1} & f_k : inlet and outlet fluxes through node (i,j,k) due to the difference matric flux potential in y direction (kg s^{-1}),
U_{i-1} &U_i: inlet and outlet fluxes through node (i,j,k) due to gravity (kg s^{-1}),
Δx, Δy and Δz : dimensions of element (i,j,k) in x, y and z directions (m),
ρ_w : water density (Mg m^{-3}), $\theta_{i,j,k}$: volumetric water content (m^3 m^{-3}),
Δt : time increment (s), and superscript t : indicates the time step.

f_i, U_i and $\theta_{i,j,k}$ all are functions of matric flux potentials (ϕ). It is required to determine values for ϕ, which makes $F_{i,j,k} = 0$ for nodes i,j,k = 1,1,1 to Mx,My,Mz (the total number of nodes). It is important to note that the values for matric flux potential, which force $F_{i,j,k}$ to zero at every node are those which assure mass balance at every node. The gravitational flux (U_i) (as a sink term) was calculated form the following equation

$$U_i = A g k_{i,j,k} = A g k_s \left(\frac{\phi_{i,j,k}}{\phi_e} \right)^{\frac{2b+3}{b+3}} \quad \text{----------(4)}$$

where: A : cross section area (m^2),
g : gravitational acceleration (9.8 m s^{-2}),
$k_{i,j,k}$: unsaturated hydraulic conductivity (kg s m^{-3}),
k_s : saturated hydraulic conductivity (kg s m^{-3}), and
ϕ_e : matric flux potential for saturated soil, which is

$$\phi_e = \frac{k_s \psi_e}{-1-(3/b)} \quad \text{----------(5)}$$

where: b : the slope of $\ln\psi_m$ vs $\ln\theta$, and
ψ_e : air entry water potential (the intercept of the best-fit line of $\ln\psi_m$ vs $\ln\theta$) (J kg^{-1}).

A new volumetric water content; $\theta_{i,j,k}$ was calculated in respect to the matric flux potentials (ϕ) as

$$\theta_{i,j,k} = \theta_s \left(\frac{\phi_{i,j,k}}{\phi_e} \right)^{\frac{1}{b+3}} \quad \text{----------(6)}$$

where: θ_s : saturation volumetric water content (m^3 m^{-3}).

Equations 2 and 4 were combined with equations 3. Appling the numerical method, the mass balance equation for node (*i*,*j*,*k*) could be approximated in Forward Finite Difference form as:

$$F_{i,j,k} = \frac{(\phi_{i,j,k} - \phi_{i-1,j,k})(x_{j+1} - x_{j-1})(y_{k+1} - y_{k-1})}{4(z_i - z_{i-1})} - \frac{(\phi_{i+1,j,k} - \phi_{i,j,k})(x_{j+1} - x_{j-1})(y_{k+1} - y_{k-1})}{4(z_{i+1} - z_i)} +$$
$$\frac{(\phi_{i,j,k} - \phi_{i,j-1,k})(z_{i+1} - z_{i-1})(y_{k+1} - y_{k-1})}{4(x_j - x_{j-1})} - \frac{(\phi_{i,j+1,k} - \phi_{i,j,k})(z_{i+1} - z_{i-1})(y_{k+1} - y_{k-1})}{4(x_{j+1} - x_j)} +$$
$$\frac{(\phi_{i,j,k} - \phi_{i,j,k-1})(z_{i+1} - z_{i-1})(x_{j+1} - x_{j-1})}{4(y_k - y_{k-1})} - \frac{(\phi_{i,j,k+1} - \phi_{i,j,k})(z_{i+1} - z_{i-1})(x_{j+1} - x_{j-1})}{4(y_{k+1} - y_k)} -$$
$$\frac{g\, k_{i-1,j,k}(x_{j+1} - x_{j-1})(y_{k+1} - y_{k-1})}{4} + \frac{g\, k_{i,j,k}(x_{j+1} - x_{j-1})(y_{k+1} - y_{k-1})}{4} +$$
$$\frac{\rho_w(\theta^{t+1}_{i,j,k} - \theta^t_{i,j,k})(z_{i+1} - z_{i-1})(x_{j+1} - x_{j-1})(y_{k+1} - y_{k-1})}{8\,\Delta t}$$

----------(7)

where: the subscripts *i* and *i*+1 refer to the two sequence nodes numbers in *z* direction, the subscripts *j* and *j*+1 refer to the two sequence nodes numbers in *x* direction, the subscripts *k* and *k*+1 refer to the two sequence nodes numbers in *y* direction,

x, *y* and *z*: distance of node in *x* direction, in *y* direction and in *z* direction, respectively in meter, and

$k_{i,j,k}$ and $k_{i\text{-}1,j,k}$: unsaturated hydraulic conductivities calculated from the corresponding node matric flux potential at the most recent iteration.

In order to get values for ϕ, which would force $F_{i,j,k} = 0$ for all nodes, the Newton-Raphson iterative method was used to solve 3-D mass balance of water flow (equation 7). The derivatives of $F_{i,j,k}$ with respect to seven matric flux potentials ($\phi_{i,j,k\text{-}1}$, $\phi_{i\text{-}1,j,k}$, $\phi_{i,j\text{-}1,k}$, $\phi_{i,j,k}$, $\phi_{i,j+1,k}$, $\phi_{i+1,j,k}$ and $\phi_{i,j,k+1}$) were calculated as following

$$\frac{\partial F_{i,j,k}}{\partial \phi_{i,j,k-1}} = -\frac{(z_{i+1} - z_{i-1})(x_{j+1} - x_{j-1})}{4(y_k - y_{k-1})}$$ ----------(8)

$$\frac{\partial F_{i,j,k}}{\partial \phi_{i-1,j,k}} = -\frac{(x_{j+1} - x_{j-1})(y_{k+1} - y_{k-1})}{4(z_i - z_{i-1})} - \frac{g\, k_{i-1,j,k}(2b+3)(x_{j+1} - x_{j-1})(y_{k+1} - y_{k-1})}{4\,\phi_{i-1,j,k}(b+3)}$$ ---(9)

$$\frac{\partial F_{i,j,k}}{\partial \phi_{i,j-1,k}} = -\frac{(z_{i+1} - z_{i-1})(y_{k+1} - y_{k-1})}{4(x_j - x_{j-1})}$$ ----------(10)

$$\frac{\partial F_{i,j,k}}{\partial \phi_{i,j+1,k}} = -\frac{(z_{i+1} - z_{i-1})(y_{k+1} - y_{k-1})}{4(x_{j+1} - x_j)}$$ ----------(11)

$$\frac{\partial F_{i,j,k}}{\partial \phi_{i,j,k}} = \frac{(x_{j+1}-x_{j-1})(y_{k+1}-y_{k-1})}{4(z_i - z_{i-1})} + \frac{(x_{j+1}-x_{j-1})(y_{k+1}-y_{k-1})}{4(z_{i+1}-z_i)} + \frac{(z_{i+1}-z_{i-1})(y_{k+1}-y_{k-1})}{4(x_j - x_{j-1})} +$$
$$\frac{(z_{i+1}-z_{i-1})(y_{k+1}-y_{k-1})}{4(x_{j+1}-x_j)} + \frac{(z_{i+1}-z_{i-1})(x_{j+1}-x_{j-1})}{4(y_k - y_{k-1})} + \frac{(z_{i+1}-z_{i-1})(x_{j+1}-x_{j-1})}{4(y_{k+1}-y_k)} +$$
$$\frac{g\, k_{i,j,k}(2b+3)(x_{j+1}-x_{j-1})(y_{k+1}-y_{k-1})}{4\phi_{i,j,k}(b+3)} + \frac{\rho_w(\theta^{t+1}_{i,j,k})(z_{i+1}-z_{i-1})(x_{j+1}-x_{j-1})(y_{k+1}-y_{k-1})}{8\,\Delta t\,\phi_{i,j,k}(b+3)}$$

---------(12)

$$\frac{\partial F_{i,j,k}}{\partial \phi_{i+1,j,k}} = -\frac{(x_{j+1}-x_{j-1})(y_{k+1}-y_{k-1})}{4(z_{i+1}-z_i)}$$ ----------(13)

$$\frac{\partial F_{i,j,k}}{\partial \phi_{i,j,k+1}} = -\frac{(z_{i+1}-z_{i-1})(x_{j+1}-x_{j-1})}{4(y_{k+1}-y_k)}$$ ----------(14)

Equations (7 to 14) constitute the basic set of Newton-Raphson equations

$$\left.\frac{\partial F_{i,j,k}}{\partial \phi_{i,j,k-1}}\right|_{\phi^t_{i,j,k-1}} (\phi^t_{i,j,k-1} - \phi^{t+1}_{i,j,k-1}) + \left.\frac{\partial F_{i,j,k}}{\partial \phi_{i-1,j,k}}\right|_{\phi^t_{i-1,j,k}} (\phi^t_{i-1,j,k} - \phi^{t+1}_{i-1,j,k}) + \left.\frac{\partial F_{i,j,k}}{\partial \phi_{i,j-1,k}}\right|_{\phi^t_{i,j-1,k}} (\phi^t_{i,j-1,k} - \phi^{t+1}_{i,j-1,k}) +$$
$$\left.\frac{\partial F_{i,j,k}}{\partial \phi_{i,j,k}}\right|_{\phi^t_{i,j,k}} (\phi^t_{i,j,k} - \phi^{t+1}_{i,j,k}) + \left.\frac{\partial F_{i,j,k}}{\partial \phi_{i,j+1,k}}\right|_{\phi^t_{i,j+1,k}} (\phi^t_{i,j+1,k} - \phi^{t+1}_{i,j+1,k}) + \left.\frac{\partial F_{i,j,k}}{\partial \phi_{i+1,j,k}}\right|_{\phi^t_{i+1,j,k}} (\phi^t_{i+1,j,k} - \phi^{t+1}_{i+1,j,k}) +$$
$$\left.\frac{\partial F_{i,j,k}}{\partial \phi_{i,j,k+1}}\right|_{\phi^t_{i,j,k+1}} (\phi^t_{i,j,k+1} - \phi^{t+1}_{i,j,k+1}) = F_{i,j,k}$$

----------(15)

The last equation was written for each node in a simulated three dimensional soil matrices under furrow and produced Mx × My × Mz equations. The equations were arranged in matrix form for order of Mx × My × Mz, which was solved by the adaptation of successive iterations Gauss-Seidel algorithm as described by Gerald and Wheatly (2003). The derivatives and F 's were evaluated at the $\phi_{i,j,k}{}^t$, and the equations solved for the $\phi_{i,j,k}{}^{t+1}$. These are then used to re-evaluate the F 's and derivatives and solved again. Convergence is determined by checking the F 's to see if they are sufficiently close to zero. The $\phi_{i,j,k}{}^{t+1}$ was used to calculate the soil moisture for each node using equation (6).

To satisfy the convergence criteria in solving the last equations of 3-D cartesian as recommended by Croft and Lilley (1977), the increment of Δt was chosen such that:

$$\Delta t \le \frac{\rho_w \theta_i\, \Delta}{6\,(b+3)\,\phi_e}$$ ----------(16)

where: θ_i : initial volumetric water content ($m^3\ m^{-3}$), and

Δ : the smallest dimension of the element (i,j,k) (m).

Discretisation and Boundary Conditions

For simulating three dimensional furrow infiltration and redistribution, a network of nodal points was first established throughout the region of furrow irrigation. 3-D region with uniform grid system in cartesian coordinates arranged throughout the domain in which soil depth was in *z* axes, furrow width was in *x* axes, and furrow length was in *y* axes as shown in figure 2. It is assumed that the nodes at and under the furrow (at $x = 0$) lie on a symmetry plane, and that another irrigation furrow lies at $2X(Mx)$, so that $X(Mx+1)$ is another symmetry plane. It is assumed that flux was zero across symmetry planes. The region was bounded by the vertical planes of symmetry midway between two adjacent furrows and through on of the furrow, and the horizontal water table at the bottom.

The boundary condition at the bottom was assumed to be set as a constant value of the matric flux potentials. If there is a water table, the matric flux potentials were set as ($\phi_{Mz,j,k} = \phi_e$) at the bottom boundary.

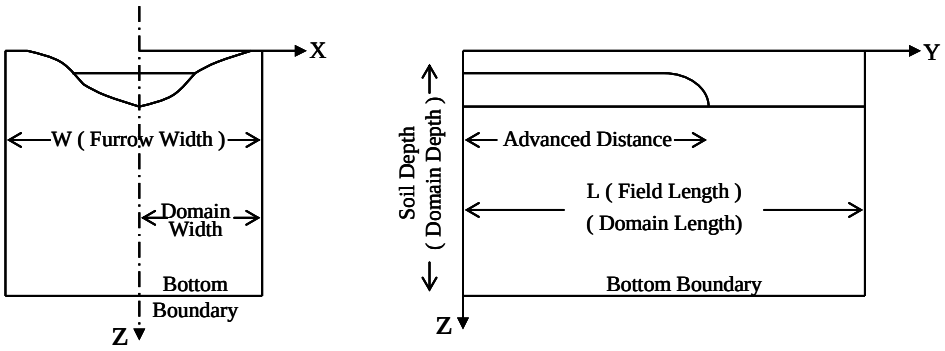

Figure 2. Schematic description of 3-D region of the model domain

Top boundary during advance and recession phases

During 3-D furrow infiltration simulation, the nodes at the wetted perimeter of the furrow were supplied by different infiltrated water (intake or fluxes) along furrow distance at time of advance trajectory. It is important to note that the supplied flux at node should be subtracted from the right hand side of the mass balance equations 3 and 7. The infiltrated

water was computed for each time increment at each wetted furrow node by

$$\delta_{i,j,k} = \frac{\Delta y \cdot W}{2\,N_d}\left\{\left[\kappa\left(t^{j+1} - \tau_{i,j,k}\right)^{\alpha} + \beta\left(t^{j+1} - \tau_{i,j,k}\right)\right] - \left[\kappa\left(t^{j} - \tau_{i,j,k}\right)^{\alpha} + \beta\left(t^{j} - \tau_{i,j,k}\right)\right]\right\} \quad \text{----------(17)}$$

where: $\delta_{i,j,k}$: nodal infiltrated water (kg s^{-1}),

t^j and t^{j+1} : elapsed time for the two sequence time increment (s),

κ : empirical coefficient of infiltration function (mm $s^{-\alpha}$),

α: empirical constant exponent of infiltration function,

β : basic intake rate (mm s^{-1}),

Δy : distance between two adjacent nodes along furrow length (m),

N_d : number of nodes bounded half wetted perimeter of the furrow,

W : furrow spacing (m), and

$\tau_{i,j,k}$: advance time (s) when water flow reaches the node i,j,k , which calculated from

$$\tau_{i,j,k} = \left(\frac{y_{i,j,k}}{\lambda}\right)^{1/r} \quad \text{----------(18)}$$

where: $y_{i,j,k}$: the node distance from the field inlet (m),and

λ and r : fitting parameters of advance trajectory function, that calculated according to Elliott and Walker (1982) as

$$r = \frac{\log(2)}{\log\left(\tau_L / \tau_{0.5L}\right)} \quad \text{----------(19)}$$

$$\lambda = L / \tau_L^{\,r} \quad \text{----------(20)}$$

where: L : total length of the furrow, and

$\tau_{0.5L}$ and τ_L : The time of advance to a point near one-half the field length and the advance time to the end field.

Equation 19 contains two unknowns, $\tau_{0.5L}$ and τ_L, a two-point advance trajectory is defined in the following procedure (Walker, 1989):

1. The first step is to make an initial estimate of the power advance exponent r value and label this value r_1.
2. Calculate the subsurface shape factor, s_z, from

$$s_z = \frac{\alpha + r(1-\alpha) + 1}{(1+r)(1+\alpha)} \quad \text{----------(21)}$$

3. Calculate the time of advance, τ_L, using the following Newton-Raphson procedure:
   a. Assume an initial estimate of τ_L as τ_{L1}

$$\tau_{L1} = 5\, A_o\, L / Q_o \quad \text{----------(22)}$$

   where: Q_o : inlet discharge per furrow ($m^3\ s^{-1}$), and
   A_o : cross-sectional flow area (m^2), which is calculated as

$$A_o = \left(\frac{Q_o\, n}{60\, p_1\, S_o} \right)^{1/p_2} \quad \text{----------(23)}$$

   where: S_o : field slope,
   n : manning coefficient, and
   p_1 and p_2 : empirical shape coefficients, which is

$$p_2 = 1.667 - 0.667\, b_2 / a_2 \quad \text{----------(24)}$$

$$p_1 = \frac{a_1^{1.667-p_2}}{b_1^{0.667}} \quad \text{----------(25)}$$

   where: a_1 and a_2 : constant and exponent of power relation between flow depth and area, and
   b_1 and b_2 : constant and exponent of power relation between flow depth and perimeter.

   b. Compute a revised estimate of τ_{L2} as

$$\tau_{L2} = \tau_{L1} - \frac{Q_o\ \tau_{L1} - 0.77\, A_o\, L - s_z\, \kappa\, \tau_{L1}^{\alpha}\, L - \left(\beta\, L\, \tau_{L1} / (1 + r_1)\right)}{Q_o - \left(s_z\, \alpha\, \kappa\, L / \tau_{L1}^{1-\alpha}\right) - \left(\beta\, L / (1 + r_1)\right)} \quad \text{--------(26)}$$

   c. Compare the initial (τ_{L1}) and revised (τ_{L2}) estimates of τ_L. If they are within about 0.5 minutes or less, the analysis proceeds to step 4. If they are not equal, let $\tau_{L1} = \tau_{L2}$ and repeat steps b through c.
4. Compute the time of advance to the field mid-point, $\tau_{0.5L}$, using the same procedure as outlined in step 3. The half-length, $0.5L$ is substituted for L and $\tau_{0.5L}$ for τ_L in Eq. 22 and 23.
5. Compute a revised estimate of r from equation 19.
6. Compare the initial estimate r_1, with the revised estimate r_2. The differences between the two should be less than 0.0001. If they are equal, the procedure for finding τ_L is concluded. If not, let $r_1 = r_2$ and repeat steps 2-6.

When water is shut off at the furrow at the furrow inlet, the flow cross sectional area begins to diminish gradually in a depletion phase until inlet

is completely dewatered. The recession time at the end field, T_{rec} was calculated using the Newton-Raphson procedure as follows:

1. Make an initial estimate of T_{rec} and label it T_{rec1};
2. Compute a revised estimate of T_{rec}, T_{rec2}:

$$T_{rec2} = T_{rec1} + \frac{\left(A_o / \upsilon W\right) - \kappa T_{rec1}^{\alpha} - \beta\, T_{rec1}}{\left(\alpha\ \kappa / T_{rec1}^{1-\alpha}\right) + \beta} \quad \text{----------(27)}$$

where: υ : recession coefficient depends on discharge and furrow shape.

3. Compare the values of the initial and revised estimates of T_{rec} (T_{rec1} and T_{rec2}) by taking their absolute difference. If they are equal to each other or within an acceptable tolerance of about .01 minutes, the value of T_{rec} is determined as the result. If they are not sufficiently equal in value, replace T_{rec1} by T_{rec2} and repeat steps 2 and 3.

The recession times along furrow length was assumed to be distributed linearly according to the following equation

$$T_{rec\,j} = T_{rec} \cdot\ y_{i,j,k} / L \quad \text{----------(28)}$$

Condition of flow arrangement

I. For continuous flow management, the infiltration has occurred over some period of time (recession – Advanced) with an application of the infiltrated water at the perimeter furrow nodes in order to simulate the distribution of water depths infiltrated along the furrow region. After the addition of water to the furrow is stopped, the water that is in wetted parts of the soil region will redistribute migrate to drier location. That executed by repeating the numerical solutions equations 7 to 15 without infiltrated water application.

II. For surged flow management, the infiltration has occurred over the first period of on-time along the first surge travel (initial wet surge zone) with an application of the infiltrated water at the corresponding perimeter furrow nodes. Then, the water that is in wetted parts of the initial wet surge zone will redistribute to drier location during the off-time period. After that, the infiltration has take place again over the second period of on-time along the second surge travel with an application of the infiltrated water at the corresponding perimeter furrow nodes, followed by redistribution of water flow during off-time period. The process is continuous until the advancing front reaches the end of the field. It is important to note that the corresponding infiltration parameter (α, κ and β) for each cycle should be used during running the infiltration and

redistribution model for each surge. The numerical method was coded in FORTRAN (Microsoft Developer Studio, 1995) for computer execution.

Filed Experimental Site

Field experiments were conducted at location of field experiment site of the Agricultural Experimental Station of Alexandria University at Abis (31° 22` N and 29° 57` E) during 2006 summer seasons. Soil samples were collected from ten different randomized locations to represent the whole experimental site. They were collected from two different soil depths in range of 0-25cm and 25-50cm. These samples were analyzed at the Soil and Water Laboratory at the Faculty of Agriculture, Alexandria University for particle size by the hydrometer and mechanical analysis to identify the soil texture. Some soil physical properties were determined such as bulk density (B.D), permanent welting point (P.W.P), field capacity (F.C), saturated moisture content (θ_s) and saturated hydraulic conductivity (k_s). Also, some soil chemical analyses such as pH, electrical conductivity (EC_e), total $CaCO_3$, organic matter (O.M) and some soluble cations (Ca^{2+}, Mg^{2+}, Na^+, and K^+) and anions (CO_3^{2-}, HCO^-, SO_4^{2-} and Cl) were determined. The electrical conductivity of irrigated water (EC_i) was 0.65 (dS/m). The physical and chemical properties were determined according to Black et al. (1982) and Klute (1986). Results of the soil physical and chemical properties are presented in Tables (1) and (2) for Abis site.

Table 1 Soil physical properties for Abis site.

Soil depth (cm)	Particle size distribution(%)			Soil texture class	B.D g cm^{-3}	θ_s m^3m^{-3}	P.W.P m^3m^{-3}	F.C m^3m^{-3}	Available Water m^3m^{-3}	k_s mm h^{-1}
	Sand	Silt	Clay							
0–25	21.23	23.19	55.58	Clay	1.27	0.578	0.251	0.398	0.147	2.08
25–50	21.15	22.89	55.96	Clay	1.30	0.563	0.275	0.405	0.130	2.11
Aver.	21.19	23.04	55.77	Clay	1.29	0.571	0.263	0.402	0.139	2.10

Table 2 Soil chemical properties for Abis site.

Soil depth (cm)	EC_e dS/m	pH	Total $CaCO_3$ %	O.M %	Soluble cations (meq/l)				Soluble anions (meq/l)			
					Ca^{2+}	Mg^{2+}	Na^+	K^+	CO_3^{2-}	HCO_3^-	SO_4^{2-}	Cl^-
0–25	2.40	7.94	27.52	1.771	10.53	3.81	16.6	0.41	-	1.21	10.21	20.4
25–50	2.12	7.93	18.80	1.326	8.32	3.11	18.1	0.51	-	1.45	12.60	16.0
Aver.	2.26	7.94	23.16	1.549	9.43	3.46	17.35	0.46		1.33	11.405	18.2

Soil Moisture Characteristic Curve

Soil water release curve for the soil of the experimental site was obtained from soil matric potential values ranging from 10 to 800 kPa. Disturbed soil samples were saturated and placed in the pressure chamber apparatus at Nubaria Research Station. At equilibrium, with no water outflow from the sample, volumetric water content at each pressure potential was determined. The resulting pressure potential; ψ and volumetric water content; θ relationship is illustrated in figure 3-a. Figure 3-b shows the relationship between matric potential; ψ and θ_s/θ for the site. The intercept with the ψ axes defined as the air entry potential; ψ_e, which was -7.208 kPa. The slope of ln ψ vs ln θ_s/θ defined as *b* values, was 9.0957.

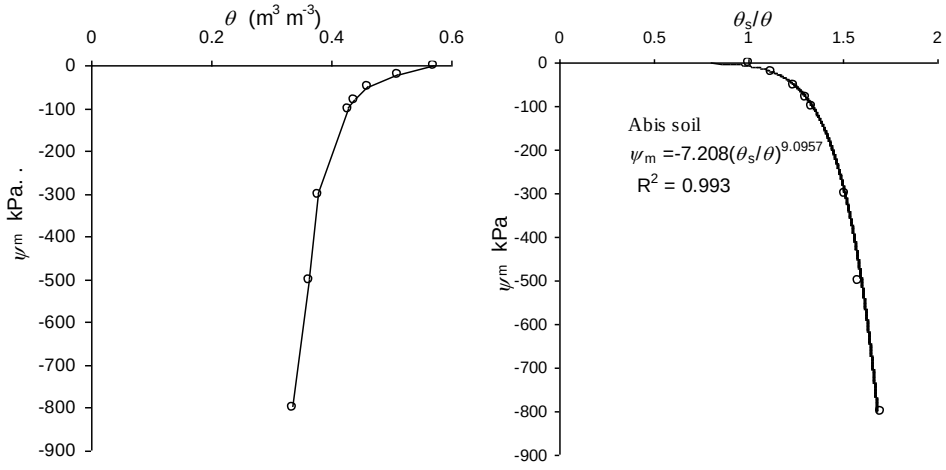

(a) **(b)**

Figure 3. (a) Typical soil moisture characteristic curve (b) the relationship between matric potential; ψ_m and θ_s/θ, for Abis site.

Experimental Design

Field area was tilled by using a disc harrow. The soil was then plowed by chisel plow twice in two perpendicular directions. The field was divided into 3 main plots to be irrigated by three different flow rates (1.45, 1.7 and 2.5 L/s). The experimental main plot area was 1012.5 m^2 (11.25 plot width × 90 m furrow length). Each plot was divided into 15 furrows (0.75 m furrow spacing), in order to have 3 replicates for the 4 treatments (three surge cycle times and continues irrigation treatments). Three furrows were used as border belt between treatments. The experimental

design was split plot design with three replicates distributed randomly. The slope in the direction of irrigation was 0.1%. For surge treatments, cycle on/off times were 5/5, 10/10 and 15/15 min.

Data Collection

The water advance and recession time were recorded at nine points at equal distances along each furrow. Infiltration parameter (κ, α and β) for both continuous and surge were determined in field by blocked furrow infiltrometer (Walker and Skogerboe, 1987). The collected data from profilemeter were used to develop a power law equation relating the area and the wetted parameter to the depth of flow, which were adapted to calculate furrow empirical shape coefficients (p_1 and p_2) according equation 24 and 25 (Walker, 1989). The values of Manning's roughness (n) were calculated according to Roth et al. (1974). Volumetric soil moistures were measured from 10, 25, 40 and 60 cm soil depth at 10, 30, 45, 60 and 80 m distance from furrow inlet after irrigation time by 1, 3, 5 and 10 days for the bare soil site. Also the soil moisture distribution was calculated from the mathematical model in a 1 cm of Δz increment (furrow depth), 1 cm of Δx increment (furrow width) and 50 cm of Δy increment (furrow length). During the water advance front to reach the end of the field, the infiltrated depths were calculated as well as the average depth of infiltration for the entire furrow. The distribution uniformity (DU) was calculated as the ratio of infiltrated depth at the end of the field to the average infiltrated depth over the entire field. The application efficiency (E_a) was calculated as the outcome of dividing the average depth of infiltration by theoretical average depth of applied water.

RESULTS AND DISCUSSION

Model Validity and Verification

Advance-recession for continuous flow

The advance time is one of the most important parameter that controls the efficiency of surface irrigation. Three sets of data were selected to be used for continuous flow validity and verification according to the flow applied to the field. The data presented in Table (3 and 4) were determined from soil and field characteristics and used as input to the model. The obtained results of continuous flow are presented graphically in figures (4-a), (4-b)

and (4-c) compared to the field data. For three inflow rates of 1.45, 1.7 and 2.6 L/s, the duration of water application for continuous irrigation were 105, 92 and 75 min and the total volume of run-off were 5.0, 6.5 and 8.5 m^3/furrow, respectively. It is clear from the figures, the model predictions are in a good agreement with the field observations. The model in some instances slightly underestimates or overestimates the recession process. The deviation can be considered reasonable limits a long the furrow's length. By comparing the model prediction with the actual field data there is a good agreement between the model prediction with field observation, for inflow rate at 1.45 and 1.7 L/s. The model for inflow rate at 2.6 L/s is slightly overestimated than the field observations. The deviation can be considered reasonable limits considering the fact that high discharge rate was used in these treatments.

Advance-recession for surge flow

Nine sets of data are used to validate and verify 3-D finite difference model for simulating furrow infiltration and redistribution water flow for surge flow condition. These are presented in Table (4). The infiltration parameters for each surge cycle were estimated from field infiltration measurements and presented in Table (3). It was observed that the maximum number of cycles, which required for the water advance front to reach the end of the field for surge irrigation at cycle time 5/5, 10/10 and 15/15 min, were 8, 4 and 4, respectively at inflow of 1.45 L/s (figures

Table (3) Infiltration coefficients for continuous and surge flow.

Cycle time	*Infiltration Coefficients	Cycle No.							
		1	**2**	**3**	**4**	**5**	**6**	**7**	**8**
Continuous	α	0.52							
	κ (mm $min^{-\alpha}$)	4.33							
	β (mm min^{-1})	0.27							
Surge 5/5 min	α	0.47	0.48	0.9	0.74	0.9	0.78	0.94	0.74
	κ (mm $min^{-\alpha}$)	2.959	1.367	0.162	0.354	0.131	0.233	0.049	0.638
	β (mm min^{-1})	0.871	0.373	0.558	0.356	0.449	0.297	0.301	0.102
Surge 10/10 min	α	0.85	0.65	0.5	0.64				
	κ (mm $min^{-\alpha}$)	0.583	0.468	0.592	0.376				
	β (mm min^{-1})	0.917	0.202	0.119	0.154				
Surge 15/15 min	α	0.7	0.84	0.83	0.96				
	κ (mm $min^{-\alpha}$)	0.917	0.112	0.135	0.027				
	β (mm min^{-1})	0.433	0.139	0.155	0.173				

*Accumulated infiltration; $Z = \kappa \tau^{\alpha} + \beta \tau$.

4-d, 5-a and 5-d). Therefore, the infiltration coefficients were estimated for that cycles numbers with respect to surge on time 5, 10 and 15 min.

The predicted results of advance and recession for surge irrigation are presented graphically in figures (4-d, e and f) and (5). The field measurements are plotted for comparison on the same figures. By comparing the model prediction with field investigation, it can be seen that the model provided a good agreement for surge flow conditions in the field. The model performed better for advance time. While, the model for recession process performed to some extent underestimates. However, the overall performance of the model is highly consistent with the field observations for the most cases. For surge flow irrigation the total volumes of water applied were substantially decreased compared to those measures for continuous flow for similar inflow rate. The duration of water application for surge irrigation at cycle time (on/off) 5/5, 10/10 and 15/15 min were 40, 40 and 60 min for inflow rates of 1.45 L/s, 35, 40 and 45 min for 1.7 L/s and 25, 30 and 30 min for 2.6 L/s, respectively. The reasons of achieving the rapid advance can be attributed to the surface seal due to the intermittent wetting and the surface hydraulic roughness of wet advance is less than dry one. Among the surge flow irrigation, the lowest volume of water application was 3.48 m^3/furrow at inflow rate of 1.45 L/s with cycle times 5/5 and 10/10 min. While, the highest application was 5.22 m^3/furrow at inflow rate 1.45 L/s with cycle time 15/15 min. The total volume of run-off for surge irrigation at cycle time (on/off) 5/5, 10/10 and 15/15 min were 0.42, 0.3 and 0.76 m^3/furrow for discharge 1.45 L/s, 0.26, 0.25 and 0.8 m^3/furrow for 1.7 L/s and 0.64, 0.79 and 0.88 m^3/furrow for 2.6 L/s, respectively.

Infiltrated depth

The cumulative intake curves were developed for a continuous and surge flow irrigation under different inflow rates at different cycle times and were plotted in figure (6). At each length increment along furrow, the opportunity time and the corresponding depth of infiltration were calculated by the model. The average depths of infiltration for entire furrow for each flow condition were estimated by the model.

For continuous flow, infiltrated depths were 7.6, 6.7 and 5.8 cm at inflow rates 1.45, 1.7 and 2.6 L/s, respectively. For surge flow at time cycles 5/5,

Table (4) Values of flow and soil parameters used in the simulation of furrow infiltration and redistribution.

Parameter	Continuous flow			Surge flow								
Inlet discharge; Q_o (L s^{-1})/furrow	1.45	1.7	2.6	1.45			1.7			2.6		
Cycle time on/off (min)	-	-	-	5/5	10/10	15/15	5/5	10/10	15/15	5/5	10/10	15/15
Field length; L (m)	90	90	90	90	90	90	90	90	90	90	90	90
Furrow spacing; W (m)	0.75	0.75	0.75	0.75	0.75	0.75	0.75	0.75	0.75	0.75	0.75	0.75
Time of cutoff (application) (min)	105	92	75	40	40	60	35	40	45	25	30	30
Field slope; S_o (m m^{-1})	0.001	0.001	0.001	0.001	0.001	0.001	0.001	0.001	0.001	0.001	0.001	0.001
Manning coefficient; n	0.038	0.039	0.038	0.037	0.036	0.037	0.035	0.037	0.034	0.036	0.038	0.039
Shape coefficient; p_1	0.363	0.4	0.3	0.42	0.45	0.339	0.432	0.438	0.399	0.376	0.402	0.369
Shape coefficient; p_2	1.74	1.85	1.9	1.82	1.75	1.79	1.69	1.74	1.85	1.86	1.81	1.77
Initial water content; θ_i (m^3 m^{-3})	0.263	0.263	0.263	0.263	0.263	0.263	0.263	0.263	0.263	0.263	0.263	0.263
Sat. hydr. conductivity k_s (mm h^{-1})	2.10	2.10	2.10	2.10	2.10	2.10	2.10	2.10	2.10	2.10	2.10	2.10
Bulk density (g cm^{-3})	1.29	1.29	1.29	1.29	1.29	1.29	1.29	1.29	1.29	1.29	1.29	1.29
Recession coefficient; υ	2	3.5	5	2	2	2	3.5	3.5	3.5	5	5	5
Element dimension; Δx (m)	0.035	0.035	0.035	0.035	0.035	0.035	0.035	0.035	0.035	0.035	0.035	0.035
Element dimension; Δy (m)	2	2	2	2	2	2	2	2	2	2	2	2
Element dimension; Δz (m)	0.05	0.05	0.05	0.05	0.05	0.05	0.05	0.05	0.05	0.05	0.05	0.05
Time increment, Δt (s)	300	300	300	300	300	300	300	300	300	300	300	300
b (Slope of $\ln\psi_m$ vs $\ln\theta$)	9.0957	9.0957	9.0957	9.0957	9.0957	9.0957	9.0957	9.0957	9.0957	9.0957	9.0957	9.0957
Air entry water potential; ψ_e kpa	-7.208	-7.208	-7.208	-7.208	-7.208	-7.208	-7.208	-7.208	-7.208	-7.208	-7.208	-7.208
Number of nodes; M_x	35	35	35	35	35	35	35	35	35	35	35	35
Number of nodes; M_y	180	180	180	180	180	180	180	180	180	180	180	180
Number of nodes; M_z	100	100	100	100	100	100	100	100	100	100	100	100

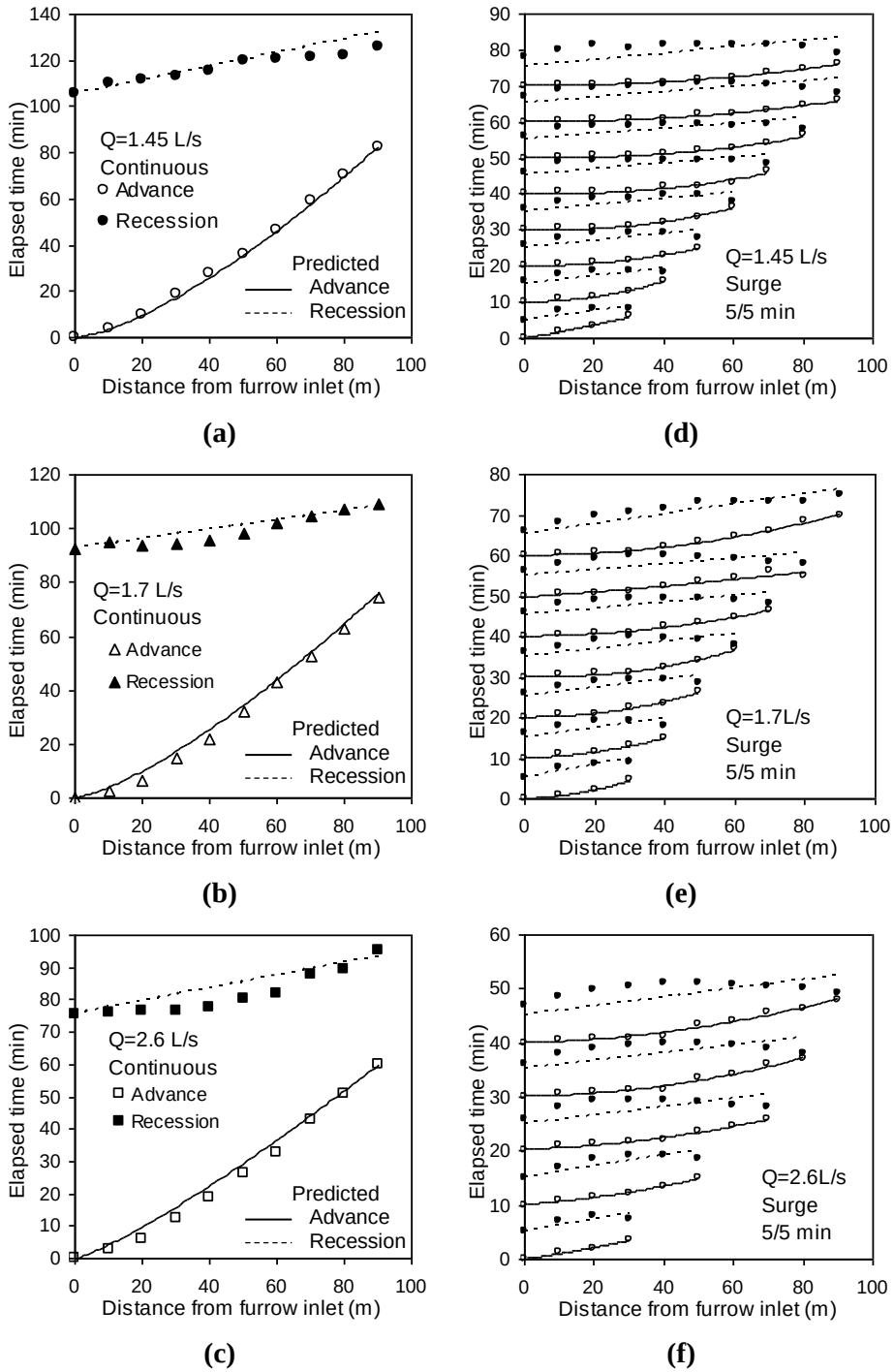

Figure 4. Predicted and observed advance and recession times at different inflow rate for continuous flow (a, b and c) and for surge flow 5/5min on/off (d, e and f)

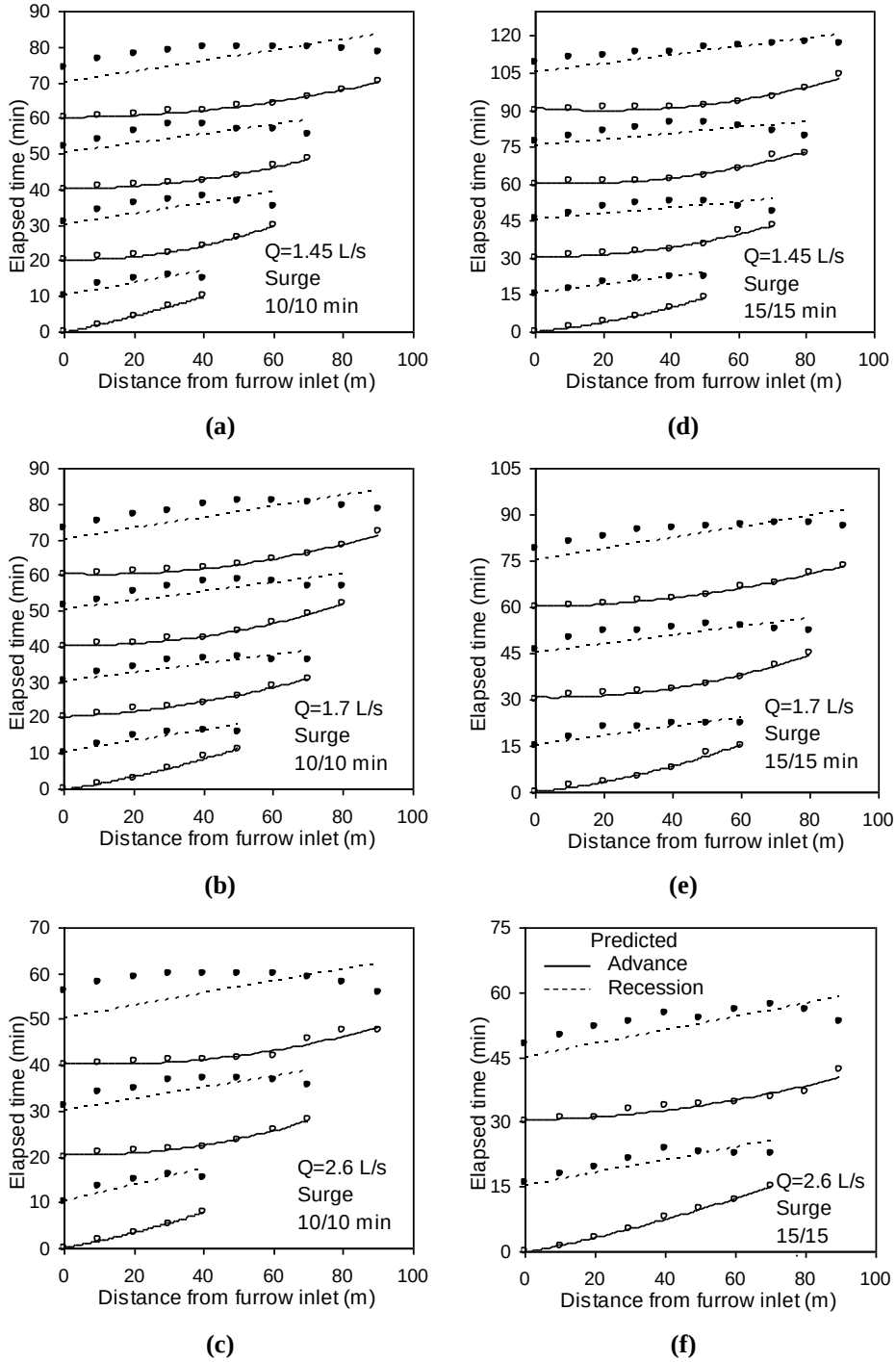

Figure 5. Predicted and observed advance and recession times for surge flow at different inflow rates and different cycle times.

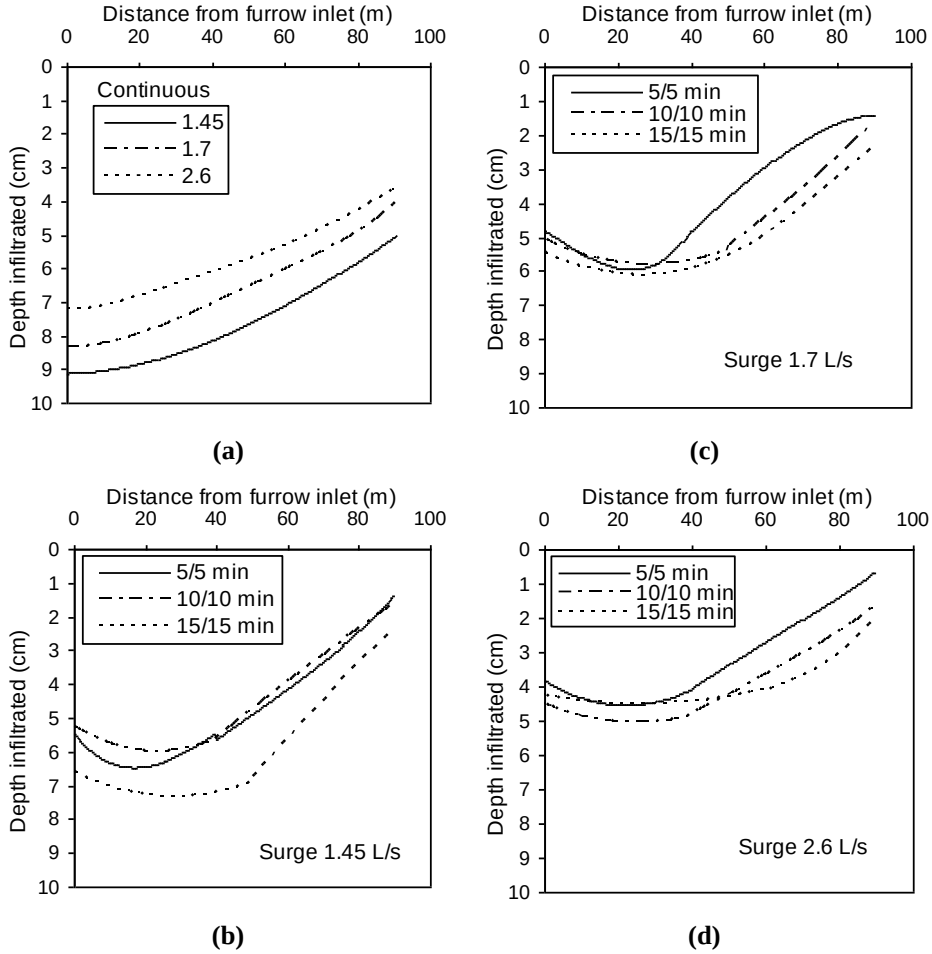

Figure 6. Predicted distribution of infiltrated water under continuous and various surge flow regimes at different inflow rates.

10/10 and 15/15 min, the infiltrated depths were 4.73, 4.56 and 5.97 cm with inflow rate 1.45L/s, 3.97, 4.7 and 5.11cm with inflow rate 1.7 L/s and 3.23, 4.04 and 4.03 cm with inflow rate 2.6 L/s. For continuous flow, Distribution uniformities (*DU*) were 66.3, 61.7 and 63.3 % at inflow rate 1.45, 1.7 and 2.6 L/s, respectively. For surge flow at time cycles 5/5, 10/10 and 15/15 min, the *DU* were 61.6, 67.9 and 53.1% with inflow rate 1.45 L/s, 57.4, 63.2 and 64 with inflow rate 1.7 L/s and 67, 68.8 and 73% with inflow rate 2.6 L/s. While, for continuous flow, the water application

efficiencies (E_a) were 56.2, 48 and 39 % at inflow rate 1.45, 1.7 and 2.6 L/s, respectively. For surge flow at cycles 5/5, 10/10 and 15/15 min, the E_a were 91.7, 88.5 and 77.5.1% with inflow rate 1.45 L/s, 75.1, 77.7 and 75.1 with inflow rate 1.7 L/s and 71, 69 and ٦9% with inflow rate 2.6 L/s.

The soil moisture distribution

The volumetric soil moistures were computed for 3-D soil domain under furrow irrigation (figure 2) for continuous and surge flow at different inflow rate and different cycle times after 1, 5 and 10 days and compared with those experimentally measured. Results indicated that there was an excellent agreement between the observed and predicted water content values. Therefore the model was used to predict soil moisture distribution along furrow distance at different furrow discharges for both continuous and surge flow regimes. Figure (7) represents the relationship between the observed and predicted values and indicates that the R^2 was 0.945 showing very close scattering for both values. This illustrates that the model used was checked and trustful to be used for next coming analysis. Figure (7) illustrates the predicted volumetric soil moisture content redistribution under furrow section for continuous flow after 1 and 5 days form irrigation with three different furrow discharges (1.45, 1.7 and 2.6 L/s). The moisture distribution contour lines were drawn for the nodes located on symmetry plane at and under the furrow (at $x = 0$) with the dimension plane of 1 m depth and 90 furrow length. The input data of the model were summarized in Table (3 and 4). The results showed in figures (8 and 9) that the soil moisture distribution in vertical plane reflects the infiltrated water pattern as water received on the furrow surface, which is shown in figure (6). It was obvious that moisture contents under continuous flow ranged between 0.40-0.26 m^3/m^3 for the three furrow inflow rates (1.45, 1.7 and 2.6 L/s) after 1 day from irrigation and ranged between 0.36-0.26 after 5 days from irrigation. The moisture content (0.26 m^3/m^3) was the initial moisture condition. So, the wetting front does not reach the soil has this moisture. As shown in figure (8), the wetting front below the inlet flow of the furrow reached to the depth of 73, 71 and 71 cm after 1 day from irrigation and 80, 79 and 79 cm after 5 days from irrigation under inflow rates of 1.45, 1.7 and 2.6 L/s, respectively. While, at the end of field, the wetting front reached to 55, 50 and 50 cm after 1

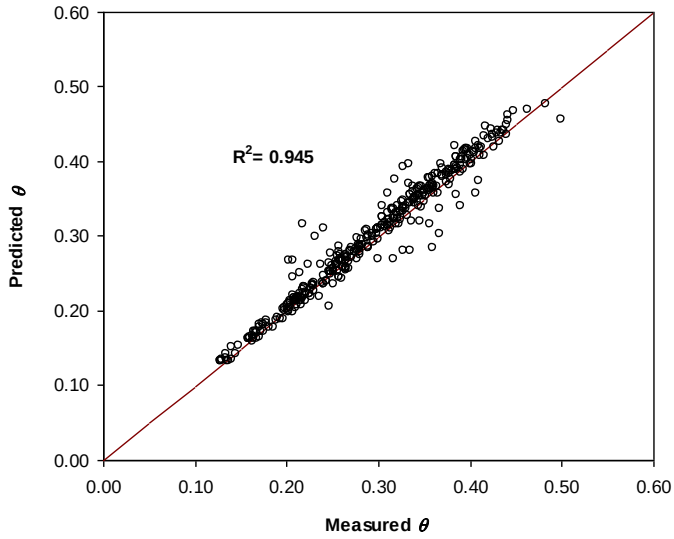

Figure 7. Relationship between predicted and measured volumetric moisture content distribution under furrow section at different furrow discharges for both continuous and surge flows.

day from irrigation and 61, 55 and 50 cm after 5 days from irrigation under inflow rates of 1.45, 1.7 and 2.6 L/s, respectively. It can be observed that for the range of soil moisture over 0.3 m^3m^{-3}, the increment of moister by one unit was occurred through 0.35 cm soil depth after 1 day from irrigation under three inflow rates. That could be expressed as the soil moisture gradient in respect to soil depth. So, the volumetric soil moister gradient in respect to soil depth was 2.85 m^{-1} after 1 day for $\theta > 0.3$ m^3m^{-3} and 1.43 m^{-1} after 5 days from irrigation for any θ. That gradient could be used to predict the soil moisture the soil profile from one point soil moisture measurement. Figure (9) shows redistribution of volumetric soil moisture, which was calculated from the mathematical mode, below furrow section for surge irrigation after 1 day form irrigation at two inflow rates (1.45 and 2.6 L/s) with the different cycle on/off times (5/5, 10/10 and 15/15 min). It is clear that the soil moisture distribution was remarkably improved along furrow length especially for the top soil layer by surge flow irrigation. Where, the wetting front moved below both inlet and end field almost by same speed. the soil moisture of 0.3 m^3m^{-3} reached the depth of 30 cm and 25 cm along 90 m furrow length after 1 day from irrigation for the inflow rate 1.45 and 2.6 L/s at different surge

time cycles. It also obvious that the high furrow inflow rate recorded high soil moisture uniformity but with low moisture content as well as low *DU* and *Ea*.

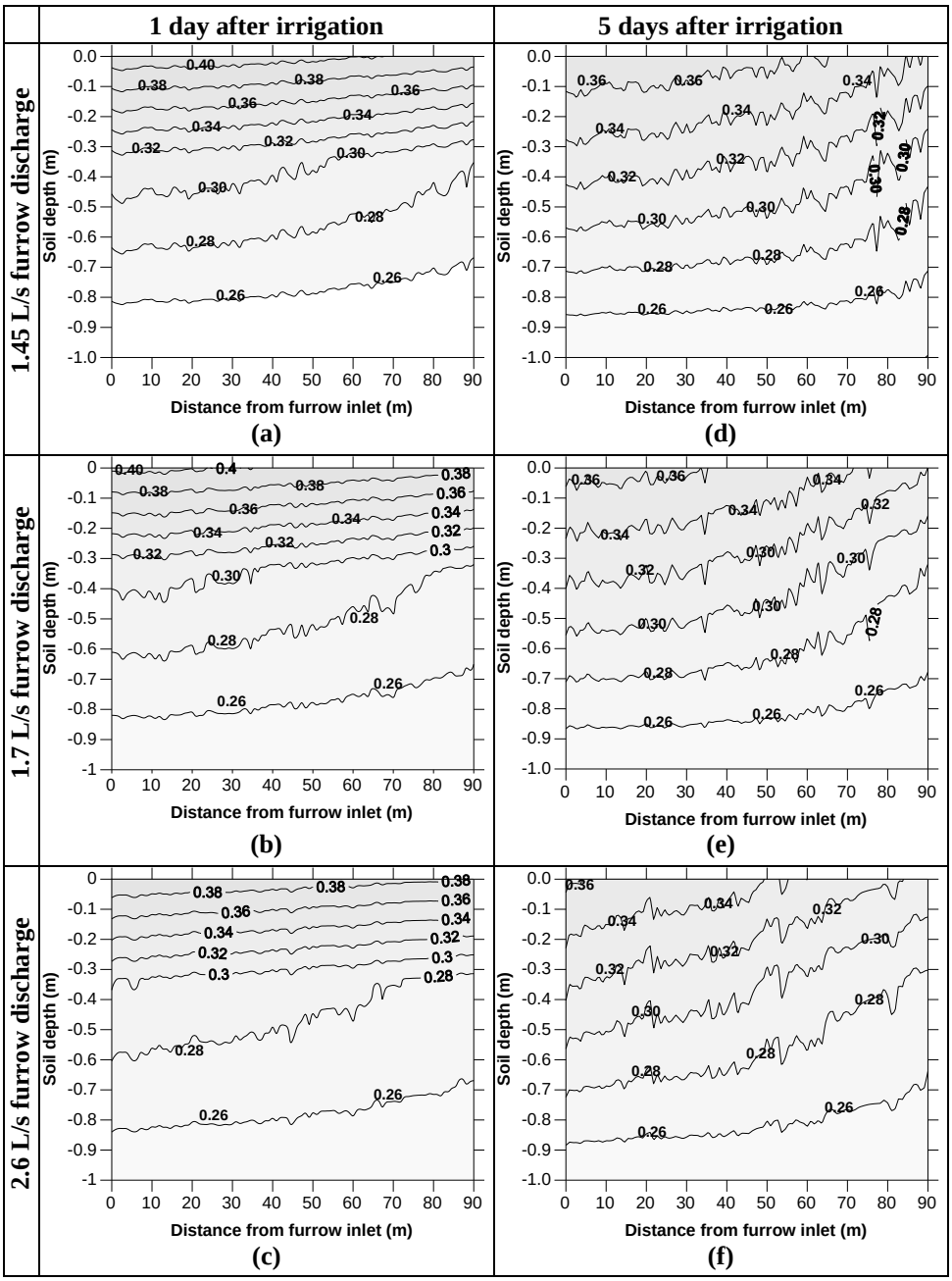

Figure 8. Soil moisture redistribution below furrow section for continuous irrigation after 1 and 5 days form irrigation at different furrow discharges.

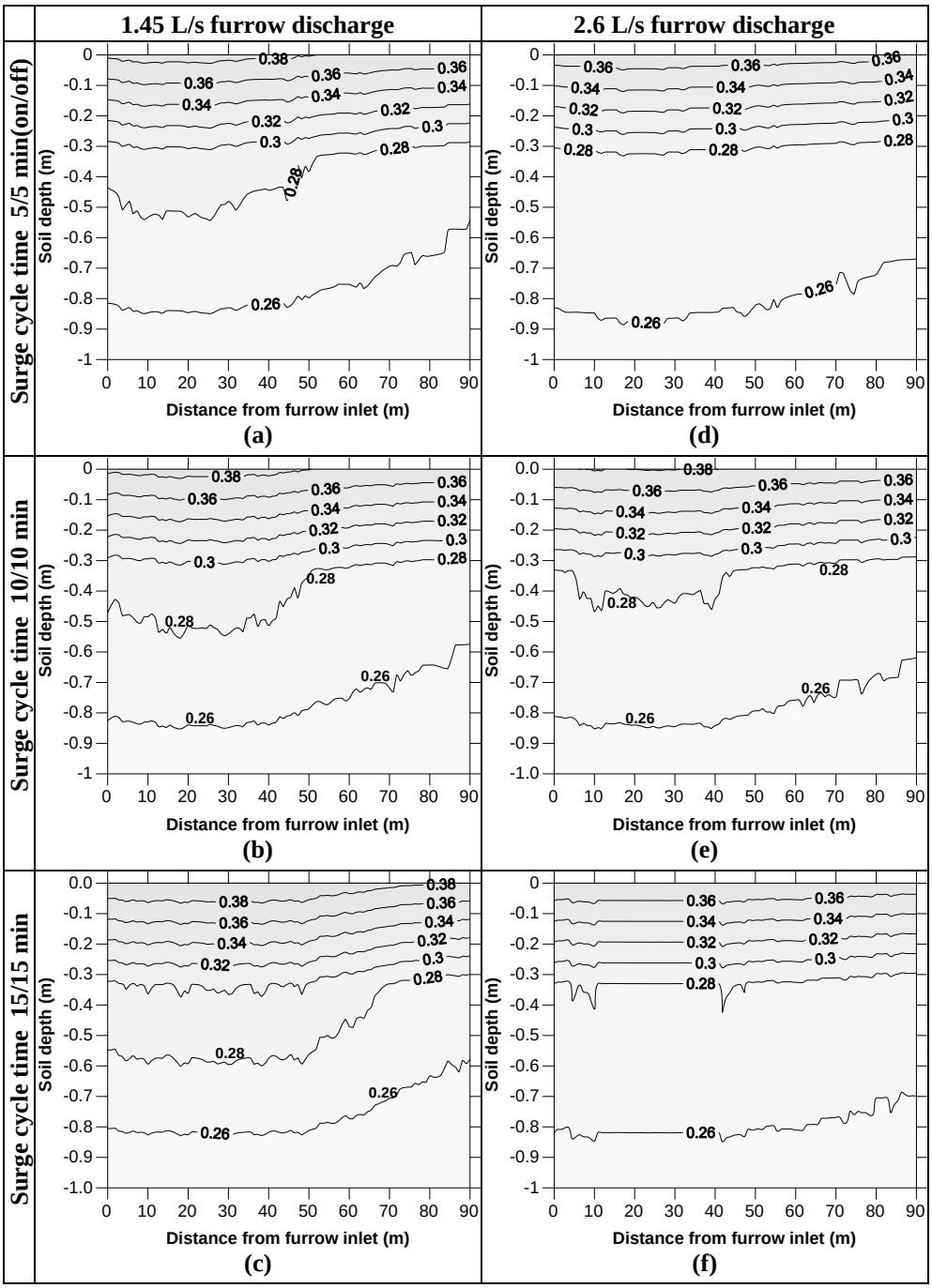

Figure 9. Redistribution of volumetric soil moisture below furrow section for surge irrigation after 1 day form irrigation at two inflow rates with different cycle times.

CONCLUSION

Based on the results obtained in this study, the following conclusions could be reached.

1. The model is capable of simulating furrow surface flow, infiltration and redistribution water flow under both continuous and surged flow management. These were validated and verified by applying the model to the field data.
2. Surge flow irrigation can provide a significant improvement in the efficiencies and uniformities of surface irrigation. It can be substantially reduced the volume of water necessary to complete the advance phase as well as infiltration rate.
3. To achieve a maximum use of the surge flow, a proper combination of the cycle time, flow rate, slope, depth of application and field length for a given soil is important. The presented model can be used effectively to analyze and determine these combinations.
4. The model accurately predicted the transient and steady soil moisture distribution under different inflow and furrow irrigation techniques.

REFERENCES

Allen, R. and J. Musick (2001). Deep ripping and blocked furrow effects on lower 1/3 furrow irrigation infiltration. Trans. ASAE 17(1):41-48.

Awady, M. N.; A. T. Ahmed; A. G. El Kabany and D. S. Moumir. (2005). Wheat response to surge irrigation. Misr J. Ag. Eng., 22(3): 811-819.

Black, C. A., D.D. Evans, L.E. Ensminger, J. L. White, F. E. Clark and R.C. Dinauer. (1982). Methods of soil analysis. 7th Printing. The Am. Soc. of Agron. Madison, Wisc., USA.

Campbell, G. S. (1985). Soil physics with BASIC: Transport models for soil-plant systems. Elsevier Sci. Pub. Co., Amsterdam. 61-97.

Childs, J., W. Wallender, and J. Hopmans (1993). Spatial and seasonal variation of furrow infiltration. J. Irrig. Drain. Eng., 119(1), 74-90.

Croft, D.R., and D.G. Lilley (1977). Heat Transfer Calculations Using Finite Difference Equations. App. Sci. Pub. Ltd. London.

Elliott, R.L. and W.R. Walker (1982). Field evaluation of furrow infiltration and advance functions. Trans. ASAE, 25(2):396-400.

Gardner,W.(1958) Some steady-state solution to the unsaturated flow equ. with application evaporation from watertable. Soil Sci.85:228-232.

Gerald, C.f. and P.O. Wheatly (2003). Applied numerical analysis. 7th Ed. Addison-Wesley Publishing Co. Inc. Menlo Park, California.

Golden Software Makers of Voxler, Strater, Surfer, Grapher, MapViewer and Didger Software (2002) surfer: contouring, girding & surface mapping. URS Corporation Mohonen, Helsinki. Finland.

Gurovich, L.A. (1992). Modeling simultaneous infiltration and surface stream advance in furrow. Presented at the 15-18 December 1992 Int. Winter Meeting by ASAE, Paper No. 922520, ASAE.

Hillel, D. (1980). Application of soil physics. Acad. Press Inc. New York.

Izuno F.T., T.H. Podmore (1985). Kinematic wave model for surge irrigation research in furrows. Trans. ASAE, 28, 1145-1150.

Kassem M. A. (2000).Comparative study for the effect of subsurface drip irrigation, surface drip irrigation and furrow irrigation systems on the growth and the yield of sunflower crop. Misr J. Ag. Eng., 17(2):319-329.

Klute. A.(ed) (1986). Methods of soil analysis. Part 1 Book series No. 9. American Soc. Of Agron. And Soil Sci. America, Madison, Wisconsin.

Mattar, M. A. (2001). Relationship between ploughing methods and surge irrigation and its effect on water rationalization. M. Sc. Thesis, Fac. of Ag., Kafer El-Sheikh, Tant. Univ., Egypt.

Microsoft Developer Studio (1995). Fortran PowerStation 4.0. Microsoft Corporation USA. S-151 Waisman Center, Madison, WI 53705–2280.

Mjelde, J.W., R.D. Lacewell, H. Talpaz and C.R. Taylor (1990). Economics of Irrigation Management. In: Management of Farm Irrigation systems. Ed.: G.J. Hoffman, T.A. Howell and K.H. Solomon. American Society of Agricultural Engineering Monograph.

Mohamed, A.I. (2007). Rational use of surface irrigation compared to drip irrigation system. M.Sc. Th., Fac.Ag., Alexndria Univ.

Oyonarte, N. A.; L. Mateos, and M. J. Palomo. (2002). Infiltration variability in furrow irrigation. J. Irrig. & Drain Eng. 128(1): 26–33.

Roth, R.L., D.W. Fonken, D.D. Fangmeier and K.T. Atchison (1974). Data for border irrigation models. Trans. of the ASAE. 17(1): 157-161.

Schwankl,W.and W.Wallender(1988).Zero inertia furrow modeling with variable infiltration and hydraulic characteristics. Trans. ASAE 31(5):

1470-1475.
Strelkoff, T. and F. Souza (1984). Modeling effect of depth on furrow infiltration. ASCE J. of Irrig. and Drain. Div. 110(IR4): 375-387.
Stringham, G.E. and J. keller (1979). Surge flow for automatic irrigation. Present at July meeting of the irrig. and drain. division, ASCE. 325-342.
Walker, W. R. and G.V. Skogerboe (1987). Surface irrigation , Theory and practice. Prentice-Hall New Jersey.
Walker, W.R. (1989). Guidelines for designing and evaluating surface irrigation systems. FAO Irrigation and Drainage, Paper 45.
Zapata, N. and E. Playan. (2000). Elevation and infiltration in a level basin: I. Characterizing variability. Irrig. Sci. 19(4): 155–164.
Zin El-Abedin, T.K. (1988). Surface Irrigation Simulation with Kinematic-Wave Model for Continuous and Surge Flow Regimes. M.Sc. Th., Fac.Ag., Alexndria Univ.
Yu, F.X. and V. Singh (1990). Analitical model for furrow irrigation. J. Irrig. Drain. Eng., ASCE, 116(2): 154-170.

الملخص العربى

نموذج ثلاثى الأبعاد لمحاكاة تسرب وإعادة توزيع مياه الرى بالخطوط

أحمد الشافعي[1]

العديد من الدراسات التي أجريت على الري السطحى إهتمت بهدروليكا الرى السطحى وكفاءة توزيع المياه معتمدة على معادلات تسرب المياه دون النظر الدقيق إلى توزيع الرطوبة تحت سطح التربة على أعماق و أزمنة مختلفة من زمن الرى، مع العلم أن تلك المستويات من الرطوبة هي التى تتحكم فى التوازن المائى بالتربة والتى تحدد مدى إتاحة المياه والعناصر الغذائية الهامة لنمو النبات كما تؤثر على معدل أداء الكائنات الحية الدقيقة والتفاعلات الكيميائية والتأثير الحرارى والتركيب الغازى تحت سطح التربة، ويرجع ذلك لصعوبة تتبع توزيع الرطوبة أثناء عملية الرى وخلال الفترة بين الريات على أعماق وأبعاد مختلفة من طول الخط ، وإنطلاقاً من هذا الهدف فقد تم بناء نموذج رياضى ثلاثى الأبعاد يحاكى تسرب وإعادة توزيع الرطوبة تحت سطح التربة على أعماق وأبعاد مختلفة على طول الخط وأزمنة مختلفة من زمن الرى تحت نظام الرى بالخطوط المستمر والمتقطع. وقد تم إستنتاج معادلات النموذج الرياضى ثلاثى الأبعاد على أساس الإتزان الكتلى ومبدأ تدفق جهد الشد الرطوبى Matric flux potential والتى قد تم حلها عدديا مستخدما طريقة الفروق المتناهية الصغر مع طريقة نيوتن رافسون لتقدير جهد الشد والمحتوى الرطوبى عند كل نقطة فى شبكة ثلاثية الأبعاد والتى تصف قطاع التربة تحت خطوط الرى. ولتقييم هذا النموذج الرياضى والتحقق من دقة توقعه بازمنة التقدم والانحسار وبالاعماق المتسربة تحت سطح التربة لاى نوع من الاراضى، تم تطوير النموذج بما يتلائم مع نظام الرى

[1] مدرس الهندسة الزراعية – قسم الهندسة الزراعية- كلية الزراعة– جامعة الإسكندرية

المتقطع والتاكد من صحة النموذج لكل من الرى المستمر والمتقطع. كذلك تم التنبؤ بكفاءة استخدام الماء باستخدام النموذج الرياضى وعمل اتزان حجمى لكمية المياة الداخلة والمتسربة والمفقودة فى الجريان السطحى والمحتوى الرطوبى تحت سطح التربة على أعماق وأبعاد مختلفة على طول الخط وذلك بعمل تجارب حقلية خلال قطاع التربة بمزرعة كلية الزراعة بمنطقة أبيس خلال الموسم الصيفى ٢٠٠٦م حيث تسود الأرض الطينية ومستوى ماء أرضى ضحل ، وقد شملت التجارب المعاملات الاتية:١- دورات لزمن فتح وغلق الماء هى ٥/٥ ، ١٠/١٠ ، ١٥/١٥دقيقة ، بالاضافة الى معاملة رى مستمر للمقارنة مع الربالمتقطع. ٢- استخدام ثلاث معدلات لتصرف الماء داخل الارض وهى : ١,٤٥ ، ١,٧ ، ٢,٦ لتر/ث.

النتائج المتحصل عليها هى :

١- من مقارنة النتائج المتحصل عليها من النموذج والنتائج الحقلية وإتضح ان النموذج يحقق ما يحدث فى الطبيعة مع اختلافات بسيطة جدا نتيجة طول الخط وذلك للرى المستمر وكانت اكثر دقة بالنسبة للرى المتقطع.

٢- وجد ان الرى المتقطع افضل من الرى المستمر وذلك لان الرى المتقطع يصل فيه الماء الى نهاية الحقل فى زمن اقل يقدر بحوالى ٢/١ـ٣/٢ زمن الرى المستمر وبذلك يتم توفير كمية الماء المستخدمة وبالتالى يحدث توفير للطاقة.

٣- رفع كفاءة استخدام الماء للرى السطحى من ٤٠٪ للرى المستمر الى اعلى من ٨٠٪ للرى المتقطع حيث انه فى الرى المتقطع نصل الى نفس العمق المتسرب من الماء تحت سطح التربة والذى يصل إليه الرى المستمر تقريبا ولكن فى الرى المتقطع نصل لهذا العمق فى زمن أقل. كما وجد أن تخفيض زمن دورة فتح وغلق الماء تزيد من كفاءة إستخدام الماء وذلك لأن زيادة الزمن للدورة تصل بالرى المتقطع إلى الرى المستمر ذو الكفاءة المنخفضة.